I&EC research
Industrial & Engineering Chemistry Research

pubs.acs.org/IECR

Article

Microcalorimetry on Cu-MCM-22 Reveals Structure−Activity Relationships for the Methane-to-Methanol Reaction

Published as part of the Industrial & Engineering Chemistry Research virtual special issue "Dmitry Murzin Festschrift".

Karoline Kvande, Moses Mawanga, Sebastian Prodinger, Bjørn Gading Solemsli, Jia Yang, Unni Olsbye, Pablo Beato, Edd Anders Blekkan, and Stian Svelle*

Cite This: *Ind. Eng. Chem. Res.* 2023, 62, 10939−10950

Read Online

ACCESS | Metrics & More | Article Recommendations | Supporting Information

ABSTRACT: With a stepwise mechanism for direct methane activation to methanol (MTM) over Cu-zeolites, it is possible to produce methanol with high selectivity. With this study, we apply adsorption/desorption experiments with *n*-propylamine, NH_3, and CH_4 as powerful techniques to learn more about the acidity and nature of the Cu-sites within a hitherto untested material for MTM, namely, MCM-22. The Cu-exchanged zeolites have a moderate performance in MTM (~0.10 mol_{MeOH}/mol_{Cu}), and upon comparing to the activity of other zeolite frameworks, we use the results found for MCM-22 to search for structure−activity relationships. We show with CO-adsorption FT-IR spectroscopy experiments that there is more than one distinct Cu-site within MCM-22, where one of which is likely linked with inactive Cu species. NH_3 adsorption/desorption experiments disclose that the Brønsted acid sites before Cu exchange are few and heterogeneous in strength, leading to a low number of C−H-activating Cu-oxo species.

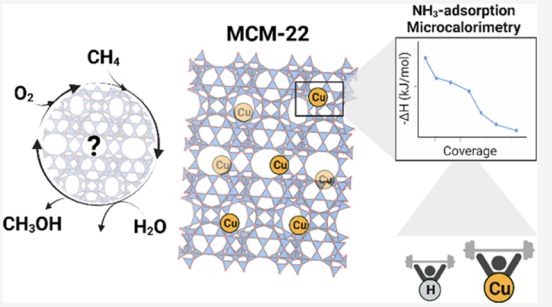

1. INTRODUCTION

As the emissions of fossil carbon and other gases leading to climate change increase, finding improved and more efficient routes for the chemical industry represents a pressing matter. One path would be to utilize more of the natural resources we already are recovering today. One of these underutilized raw materials is methane. Since gas is expensive to transport from remote areas, finding a path for directly converting methane into a liquid, like methanol, without the need for creating synthesis gas (CO and H_2) would be of great potential for the industry.[1] Several different routes have been suggested over the years; however, one of the more promising routes was suggested by Groothaert et al. back in 2005.[2] They showed that dimeric Cu-oxo species formed in ZSM-5 were able to activate the C−H bond in methane to form methanol. The type of reaction proposed is a cyclic reaction route that involves a high-temperature step in an oxidizer, e.g., oxygen at ~500 °C, forming Cu_xO_y-moieties in the zeolite framework. Methane is then dosed onto the sample at around 200 °C at which point some of the Cu-sites are reduced to Cu^+ by the formation of methoxy species. Finally, methanol is extracted by passing steam through the reactor bed. With this method, very high selectivity is achieved because the stepwise nature of the reaction protocol hinders the gas-phase reaction between reactants and products and hence avoids overoxidation of the products. Since Groothaert et al., many different Cu-loaded zeolite frameworks have been tested for this reaction, with some of the more promising being MOR,[3−8] CHA,[9,10] FER,[11] FAU,[12] and MAZ.[13] Although many different frameworks have already been tested, there are still unresolved questions regarding the effect of the morphology, acidity, and homogeneity of the ion exchange site on the formation of the active Cu-sites and hence the material's activity toward methanol. With that in mind, we aimed to investigate MWW, more specifically, MCM-22, a hitherto untested material, for the methane-to-methanol (MTM) reaction. For other reactions, MCM-22 has been tested extensively as a large-pore zeolite for methylation reactions.[14,15] MCM-22 has an MWW-type framework with 10-ring pore openings and two independent channels.[16] One channel is a sinusoidal 10-ring channel, while the other consists of layered super cages with 12-ring diameter, interlinked by double 6 rings, and accessible through 10 rings. The channel and cage sizes are not that different from, e.g., MOR, FAU, and MAZ zeolites that also have 12-ring pores, and MCM-22 often has properties similar

Received: March 27, 2023
Revised: June 15, 2023
Accepted: June 23, 2023
Published: July 7, 2023

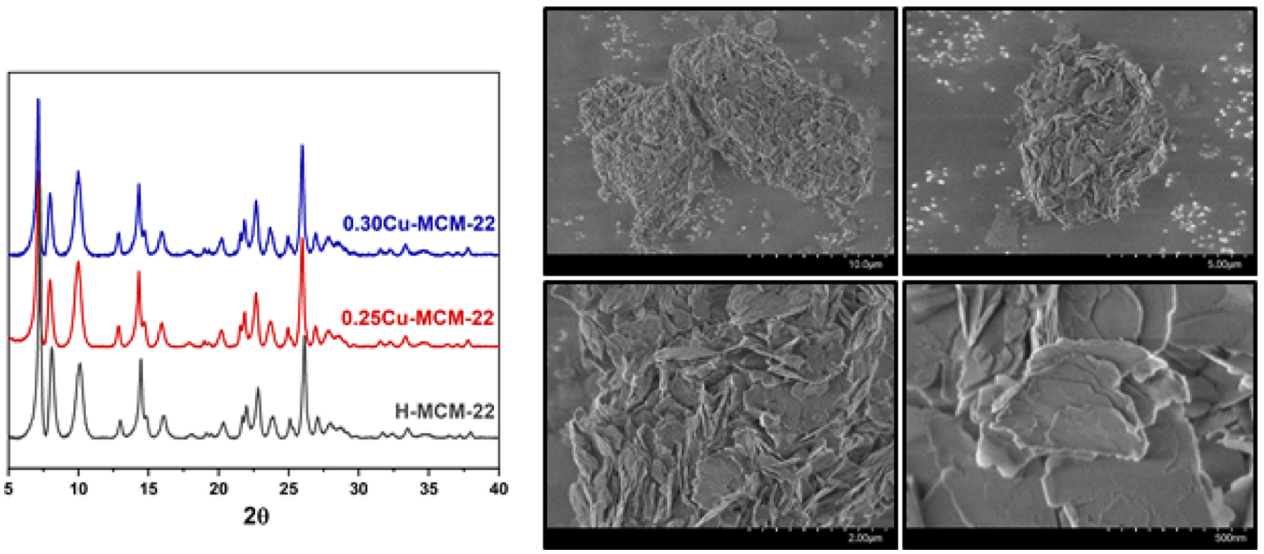

Figure 1. PXRD patterns (left panel) of the three MCM-22 samples. The patterns are organized from bottom to top in the order of increasing Cu content. SEM images (right panel) of 0.25Cu-MCM-22. The four images show the crystal agglomerates of 0.30Cu-MCM-22 at different scales.

Table 1. Summary of Synthesis, Characterization, and Test Results of the Different Ion-Exchanged MCM-22 Zeolites Discussed Herein[a]

sample name	exchange conditions[b]	elemental analysis			specific surface area (m^2/g)[c]	water content (%)[d]	MTM test results		
		Si/Al	Cu/Al	Cu (μmol/g)			yield (μmol/g)	productivity (mol_{MeOH}/mol_{Cu})	selectivity (%)
H-MCM-22		15.0			540	10			
0.11Cu-MCM-22	LIE, 0.001	15.3	0.11	116	n.d.	n.d.	5	0.04	44
0.25Cu-MCM-22	LIE, 0.01	15.2	0.25	263	n.d.	10	20	0.08	77
0.29Cu-MCM-22	LIE, 0.0075	15.8	0.29	286	n.d.	n.d.	34	0.12	75
0.30Cu-MCM-22	LIE, 0.02	15.2	0.30	311	n.d.	10	27	0.09	76
Cu-MCM-36	LIE, 0.005	18.5	0.24	208	n.d.	n.d.	10	0.05	67
Cu-ITQ-2	LIE, 0.005	15.4	0.20	205	n.d.	n.d.	12	0.06	71

[a]The elemental composition was obtained with MP-AES and is reported as Si/Al, Cu/Al, Cu (μmol/g), and Cu wt %. [b]Both the exchange method and molarity of the exchange solution are indicated here. [c]Specific surface area is obtained by N_2-physisorption experiments. [d]Water content obtained by TGA.

to 12-ring zeolites.[17] However, one main difference is the complexity of the MCM-22 structure, causing the zeolite to have no less than eight different T-sites, while the others have 4, 1, and 2, respectively. Additionally, MCM-22 has an outer surface that consists of pockets formed by half a super cage. These pockets have been shown to hold some of the catalytic sites of MCM-22.[18]

As the complex structure especially could influence the positioning of the Brønsted acid sites, and by extension the Cu speciation, it was crucial to assess the acidity of the zeolite, with and without Cu. To that end, NH_3 microcalorimetry, a powerful technique providing information on the heats of adsorption of various acidic sites as well as the adsorption isotherms was applied to study the H- and Cu-MCM-22. Cu-exchanged MCM-22 was synthesized, characterized, and tested for the MTM reaction. Furthermore, CO-adsorption experiments with Fourier transform infrared (FT-IR) and X-ray absorption spectroscopy (XAS) was used to assess the nature of the Cu-sites beyond information obtained from basic characterization tools. NH_3- and *n*-propylamine temperature-programmed desorption (TPD) experiments were then used in comparison to the NH_3-microcalorimetry to investigate the strength and homogeneity of the active sites by comparing Cu- and H-exchanged MCM-22. Lastly, CH_4-calorimetry experiments were attempted to learn more about the C−H activation and adsorption process in that step of the MTM reaction protocol.

2. RESULTS AND DISCUSSION

2.1. Material Properties of H- and Cu-MCM-22. MCM-22 was synthesized in-house and Cu-exchanged by liquid ion exchange with Cu acetate. Four samples with varying Cu content were prepared, ranging from 0.11 to 0.30 Cu/Al. For naming the materials, the following code has been applied; *xy*-MCM-22, where *x* is the Cu/Al ratio and *y* is either H or Cu. To explore the structural effect on the MTM activity, two 2D materials with the MWW framework were also prepared and tested. ITQ-2 is a delaminated material, where the MCM-22 structure is cut in a plane going through the middle of the supercage. MCM-36 is similar to ITQ-2, but the planes are held together with silica pillars. To verify that the materials were pure and well exchanged, they were characterized with a suite of different techniques like microwave plasma atomic emission spectroscopy (MP-AES), powder X-ray diffraction (PXRD), scanning electron microscopy (SEM), thermogravimetric analysis (TGA), and N_2-physisorption (for experimen-

https://doi.org/10.1021/acs.iecr.3c00988
Ind. Eng. Chem. Res. 2023, 62, 10939−10950

tal details, see the Supporting Information, Sections S1−S4). The PXRD pattern of H-MCM-22 was refined against the MWW crystal structure (Figure S1), and the result demonstrated that a pure MCM-22 zeolite crystal structure was retained. In Figure 1, we report the comparison of H-MCM-22 to two of the Cu-exchanged samples, and no peaks related to larger Cu nanoparticles and agglomerates are observed in the PXRD pattern. The synthesized MCM-22 material had a typical morphology with the crystals growing in the form of small, layered sheets packed together in larger, "rose-like" agglomerates.[19]

All physicochemical data of all the MCM-22 materials as well as the ITQ-2 and MCM-36 are reported in Table 1.

2.2. Performance in the Methane-to-Methanol Reaction. The Cu-exchanged MCM-22 materials were, to the best of our knowledge, evaluated herein as hitherto untested materials for the MTM reaction. The reaction protocol is based on an optimized protocol by Pappas et al. on Cu-CHA.[9] The materials are first activated at 500 °C in O_2 (8 h), cooled to 200 °C, flushed with He (45 min), and exposed to CH_4 (3 h). Then, the sample is again flushed with He (45 min), before steam (10% H_2O in He), at the same temperature, and is passed over the material to extract the products. The results from the tests are reported in Table 1, while the productivity and selectivity are visualized in Figure 2. The total production

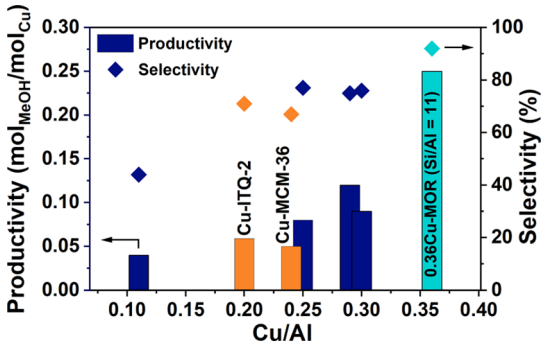

Figure 2. Performance data obtained over Cu-MCM-22 using the following protocol: 8 h in O_2 (500 °C), He at 200 °C (45 min), followed by CH_4 (3 h), He (45 min), and steam extraction (10% H_2O in He). Bars represent the productivity (mol$_{MeOH}$/mol$_{Cu}$), while the diamonds represent the selectivity (%). MCM-22 with four different Cu loadings are given in blue, the 2D materials (ITQ-2 and MCM-36) are given in orange, and for comparison, a previously reported Cu-MOR zeolite is plotted in cyan.[21]

of methanol is normalized to the Cu content (productivity, mol$_{MeOH}$/mol$_{Cu}$). Selectivity is given in % and reports the amount of methanol obtained compared to the total effluent measured during the desorption with steam, where the byproduct of the reaction was CO_2. When comparing the productivity, it is clear that the sample with very low Cu content (Cu/Al = 0.11) has a lower production of methanol per Cu-site than the other three MCM-22 materials. The low productivity observed over the low Cu-loaded sample suggests that the most active sites are not sufficiently occupied at such a low loading. This is also reflected by the lower-than-normal selectivity toward MeOH (44%). We speculate that copper atoms are spaced too far apart at this low loading to form the active multimeric Cu-oxo species. The other three samples appear to level out at a productivity of around 0.10 mol$_{MeOH}$/mol$_{Cu}$, no matter if the Cu content is increased, indicating that a plateau is reached. When comparing the values obtained herein to other tested Cu-zeolites for methane to methanol (e.g., the Cu-MOR that is provided in Figure 2 for comparison), the values are lower than what is reported herein, when using the same reaction protocol and setup. Depending on the framework, exchange method, Si/Al, and Cu/Al ratio, the productivities previously obtained for Cu-zeolites are in the range of about 0.10−0.47.[9,11,20] The selectivity toward methanol of *x*Cu-MCM-22 was about 75% for the three most productive samples. This is also in the lower region of what is typically observed with this reaction protocol over other Cu-zeolites.[9,11,20]

Furthermore, we also prepared delaminated MCM-22, known as ITQ-2 where the supercage is removed, leaving only the surface pockets and the sinusoidal channel. Similarly, MCM-36 has the same topological features except for silica pillared between the layers. Both materials had comparable Si/Al ratios and Cu/Al ratios of 0.20 and 0.24. The MeOH productivity did not increase above 0.06, comparable to the 0.11Cu-MCM-22 sample at low loading. This finding suggests that the most productive sites likely require the structural confinement of the 3D material and lie somewhere in the supercage. These structural differences opened up for further analysis of some of the samples to search for structure−activity relationships.

It is worth mentioning here that MCM-22 has also been shown previously to be quite active for the methanol-to-olefin (MTO) reaction by exhibiting a high selectivity toward propene.[22] In the MTO mechanism, there are generally two pathways suggested for methylation, a concerted and a stepwise route.[23] The latter leads to the formation of a methoxy intermediate; however, due to the complex channel structure of MCM-22, it is still debatable which of the mechanisms is dominant in this material.[24] A stepwise mechanism could indicate that the material can form and stabilize methoxy species at least on Brønsted sites, which do suggest that the material should be a candidate for the MTM reaction. Since our material characterization presented above indicate that the materials have been properly synthesized and exchanged with Cu, it became obvious that more investigations were needed to understand the reason for the low methanol production of these materials compared to other Cu-exchanged zeolites.

For further analysis, the H-MCM-22 material was chosen together with the two Cu-exchanged samples with similar methanol productivity but the most significant difference in Cu-loading.

2.3. Employing XAS and FT-IR Spectroscopy to Study the Nature of the Cu-Sites. *2.3.1. Investigating the Oxidized State of Cu after Activation.* It has previously been shown that a pure Cu^{2+} state is important before methane loading to get the highest MTM performance possible. It was therefore essential to investigate the oxygen-activated state of the Cu-exchanged materials with XAS. In Figure 3, we report the results obtained over activated samples sealed in capillaries. Both the XANES and EXAFS correspond well with an almost pure Cu^{2+} state as there is no evidence for the spectral features of Cu^{+}. A detailed description of the relevant features is reported in the Supporting Information, Section S5.

The spectral features of the two samples investigated are very similar. A slightly higher white line and first shell peak are observed in the XANES and FT-EXAFS spectra for 0.30Cu-MCM-22. This could indicate a marginally higher coordination

https://doi.org/10.1021/acs.iecr.3c00988
Ind. Eng. Chem. Res. 2023, 62, 10939−10950

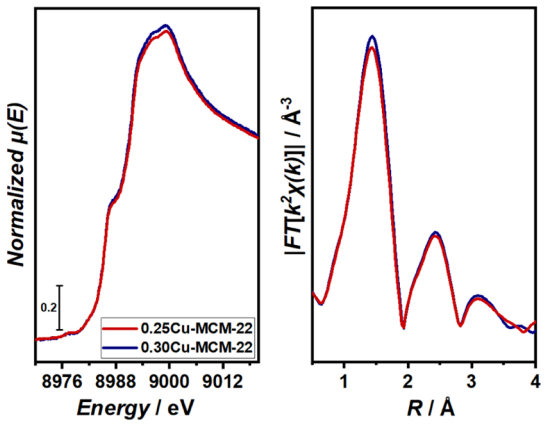

Figure 3. XANES (left panel) and FT-EXAFS (right panel) spectra of the two Cu-exchanged MCM-22 samples, 0.30Cu-MCM-22 (blue) and 0.25Cu-MCM-22 (red). The spectra are obtained at RT on capillaries activated at 500 °C in air overnight and sealed at high temperature.

number around the Cu atoms as well as more uniform bond lengths in this sample. Such trends have previously been suggested to be correlated with higher methanol productivity; however, the difference is so small herein that such a correlation should not be ascertained without a deeper investigation.[21]

2.3.2. CO-Adsorption on Cu^+ Sites with FT-IR Spectroscopy. To understand more about the effect of the zeolite structure on the Cu-speciation, the samples were first treated by activating in vacuum to induce "self-reduction" of the Cu-sites to Cu^+[25,26] and then probed with CO at RT during FT-IR spectroscopy measurements. This has shown to be a helpful tool in studying the Cu-sites of zeolites.[11,27,28] At room temperature, it is only Cu^+-carbonyl species that are stable enough to be observed in an FT-IR spectrum. In Figure 4, we show the region of interest (2250−2080 cm^{-1}) from the experiments. 0.25Cu-MCM-22 can be seen in Figure 4a, while 0.30Cu-MCM-22 is shown in Figure 4b. 0.30Cu-MCM-22 is

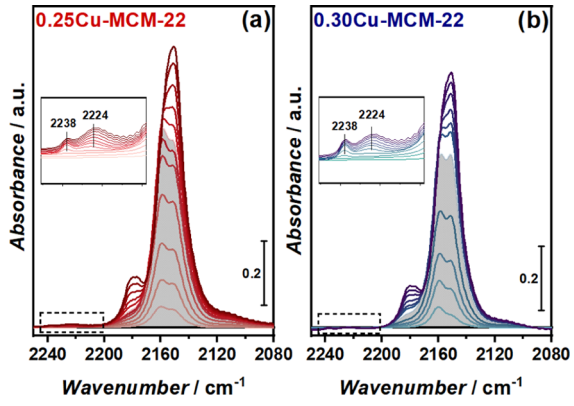

Figure 4. FT-IR spectra of the −CO stretch region after exposure to CO of the two Cu-exchanged MCM-22 samples, 0.30Cu-MCM-22 (blue) and 0.25Cu-MCM-22 (red). The spectra are collected at RT after stabilization of the equilibrium pressure at incremental doses of CO from ∼50 μbar to 8 mbar. The samples were pretreated in vacuum at 450 °C (1.5 h). The spectra are background-subtracted by dividing on the pretreated spectra and normalized to the framework overtone, as well as Cu content. The insets give a closer view of the marked area where the CO vibrations on Al^{3+} are found.

the sample with the highest Cu-loading and slightly higher productivity. Looking at both samples, it is clear that as CO is dosed initially, two bands appear at 2158 and 2151 cm^{-1}. While only one band is usually observed for Cu^+-monocarbonyl species in Cu-zeolites, for Cu-loaded MCM-22, two distinct bands are growing.[11,27−29] This has also been seen for Cu-BEA zeolites.[29] The two distinct bands indicate that, in MCM-22, there are at least two structurally different Cu-sites, which is coherent with the sample having at least three major positions for Cu to be positioned, namely, the sinusoidal 10-ring channel, within the supercage, or on the external surface in the supercage half-cups. Interestingly, at low CO coverage, in 0.30Cu-MCM-22, there seems to be more CO interacting with the Cu species, giving rise to the high wavenumber band (2158 cm^{-1}) relative to the band at 2151 cm^{-1}, while in 0.25Cu-MCM-22, the intensities of these bands are more similar. When the CO dosage increases to almost full monolayer coverage (marked by the gray area in Figure 4), the opposite trend is observed for the two samples. The fact that the sample with the lowest Cu/Al ratio has a higher band intensity of the high-frequency band at monolayer coverage has also been observed previously by Frolich et al.[30] They correlate the high-frequency band to a trigonal planar Cu^+ species coordinated to two framework oxygen and one CO molecule. The low-frequency band, however, is a bit more uncertain, but they suggest it be linked to a higher coordinated Cu species. The authors also observe that this band diminishes as the temperature is increased, suggesting that the Cu^+ species shift to a trigonal planar configuration. The authors indicate that the low-frequency band is in a more constrained position, possibly at the double 6-ring at the bottom of the supercage, while the high-frequency band comes from a species situated at the center of the supercage.

As the CO dosage is increased beyond monolayer coverage, three new bands start appearing corresponding to the symmetric and asymmetric stretches of dicarbonyl species interacting with Cu^+. The symmetric stretch is observed as two separate bands, corresponding to the two structurally different sites at 2180 and 2176 cm^{-1}. The asymmetric stretch, however, is observed as a small downward shift and merging of the monocarbonyl bands into a more single narrow band at about 2151 cm^{-1}. Few differences are observed for the two samples as the dicarbonyl species are formed, suggesting that the availability for dicarbonyl formation is about the same in the two Cu-exchanged samples.

In addition to the typical bands appearing for CO interacting with Cu^+, there are also two smaller bands appearing at slightly higher wavenumbers (2238 and 2224 cm^{-1}). These bands are positioned at typical energies for CO interacting with extra-framework Al^{3+} (EFAl) sites.[32,33] The observation of these bands suggests that there is some extra-framework Al in the zeolite, which reduces the amount of Brønsted sites able to form in the sample. This could have at least two potential implications on the MTM reaction. First, fewer Brønsted sites could minimize the amount of Cu exchanged in the samples. Indeed, LIE with both 0.01 and 0.02 M $Cu(OAc)_2$ solutions led to very similar amounts of Cu exchanged. Although other methods to increase the Cu exchange were not attempted as higher loadings often lead to Cu clusters and nanoparticles, the similarity between the two materials obtained with different LIE solutions suggests that we have reached a maximum of Cu exchange sites. Second, it has been shown that the presence of Brønsted sites is important for stabilizing methoxy inter-

https://doi.org/10.1021/acs.iecr.3c00988
Ind. Eng. Chem. Res. 2023, 62, 10939−10950

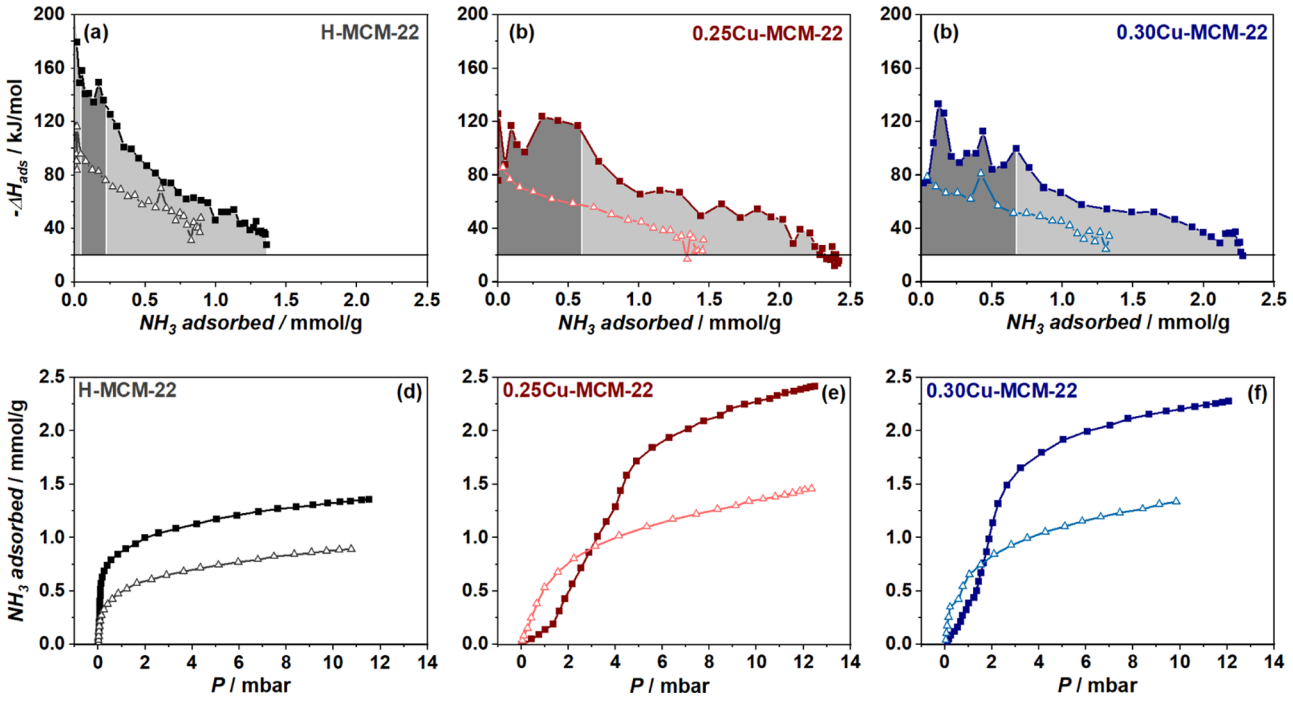

Figure 5. Differential heats of adsorption (a−c) and adsorption isotherms (d−f) for NH_3 on the three MCM-22 samples (a−c). Both primary (dark color, filled symbol) and secondary (light color, open symbol) heat of adsorption curves and adsorption isotherms are reported. The differential heats of adsorption (kJ/mol) are plotted against the NH_3 adsorbed in μmol/g. The sharp horizontal line represents the enthalpy for NH_3 condensation. The adsorption isotherms are given as adsorbed NH_3 in μmol/g per absolute pressure (mbar).

mediates, and if the accessibility to the remaining sites is somewhat blocked by the EFAl, this could both minimize the availability for Cu exchange and also reduce the stabilizing effect of Brønsted acid sites. Based on this, we found it interesting to further investigate the effect of acid site distribution in the MCM-22 framework and, by extension, its effect on the Cu siting to unravel more about the influence these parameters have on the MTM reaction.

2.4. NH_3-Adsorption Microcalorimetry. To study the changes in acidic properties of MCM-22 before and after Cu exchange, NH_3-adsorption microcalorimetry experiments were performed. NH_3 was initially chosen as the probe molecule since both Brønsted and Lewis acid sites should adsorb the NH_3 molecule. The heat evolved during adsorption should give some insight into the strength of the adsorption site as well as the heterogeneity of the acid sites. The results are reported in Figure 5. In the top panel, we show the differential heat of adsorption (ΔH_{ads}) versus the amount of adsorbed NH_3, obtained for H-MCM-22 (a), 0.25Cu-MCM-22 (b), and 0.30Cu-MCM-22 (c). Both a primary (solid squares) and a secondary (open triangles) adsorption experiment were performed for all three samples. If we first look at the differential heat of adsorption measured for the Cu-free sample, there are three regions of interest marked with alternating light- and dark-gray colors. Initially, at very low coverage, there is a strong heat of adsorption (>160 kJ/mol), which decreases sharply as the coverage increases. This is typically related to strong Lewis acid sites.[34] The second region of interest is a narrow area (−150 kJ/mol < −120 kJ/mol) that should be correlated with a set of homogeneous acid sites like the Brønsted acid sites.[34] The Al concentration of the H-MCM-22 applied herein is about 1.1 mmol/g, and as the second region diminishes already at about 0.25 mmol/g of adsorbed NH_3, it is evident that the amount of homogeneously strong Brønsted acid sites is lower in this sample, compared to what would be expected from a zeolite with similar Al content. Indeed, this area has previously been reported to be stable up to at least 0.8 mmol/g in an H-MOR with similar Al content (1.1 mmol/g) as our samples.[35] After the high enthalpy area, we enter the third region, where the heat of adsorption decreases gradually with coverage until the enthalpy for condensation of NH_3 is reached (ΔH_c = −23.4 kJ/mol). This is linked with a set of heterogeneous acid sites,[34] indicating that a large portion of the total amount of Al in the sample is either present as EFAl, as indicated already by FT-IR spectroscopy, or more Brønsted sites with lower heat of adsorption possibly due to lower accessibility.

If we shift our focus onto the Cu-exchanged samples, a few interesting changes are noteworthy. The first and second regions of strongly adsorbing sites and Brønsted acid sites seem to be nonexisting. However, a broader region of heterogeneous sites is observed in a region of intermediate strength with ΔH_{ads} between −120 and −80 kJ/mol. This region is observed up to about 0.6 mmol/g of adsorbed NH_3 for 0.25Cu-MCM-22 and almost 0.7 mmol/g for 0.30Cu-MCM-22. The "spikes" or heat fluctuations observed in this region can be speculated to be due to the oxidation of NH_3 from a reaction with the preoxidized Cu species. This would release additional heat and influence the heat of adsorption measured.[36] Such fluctuations have also been observed previously on a different system by Arrigo et al.[37] The oxidation of NH_3 would also lead to some of the Cu-sites being reduced to Cu^+. Giordanino et al. propose a possible reaction pathway at low temperatures (120 °C) that involves the oxidation of two NH_3 molecules to N_2 and H^+, and this reaction provides the electrons needed for the reduction of Cu^{2+} to Cu^+.[38] They further suggest that the reduced Cu-sites could interact with NH_3 molecules to form mobile, linear

https://doi.org/10.1021/acs.iecr.3c00988
Ind. Eng. Chem. Res. 2023, 62, 10939−10950

Table 2. Density of Acid Sites Obtained by *n*-Propylamine TPD and NH_3-TPD Together with the Irreversible NH_3 Adsorbed Measured by Calorimetry[a]

sample name	Al concentration (mmol/g)	Cu concentration (mmol/g)	acid site concentration from *n*-propylamine TPD $C_{3=}$ (mmol/g)	acid site concentration from NH_3 TPD NH_3 (mmol/g)	irreversible NH_3 adsorption from calorimetry NH_3 (mmol/g)
H-MCM-22	1.07		0.66	0.57	0.44
0.25Cu-MCM-22	1.03	0.26	0.51	0.64	0.82
0.30Cu-MCM-22	1.03	0.31	0.46	0.76	0.84

[a]The Al and Cu content is also reported for comparison.

diammine Cu^+ complexes. The formation of Cu^+ and the mobility of diammine Cu^+ complexes would introduce structural rearrangements, which again could influence the differential heats measured during adsorption.

Since the strong Lewis and Brønsted site enthalpy region is nonexisting in the Cu-exchanged samples, we conjecture that Cu is exchanged first with the strongest Brønsted sites, as well as a few strong Lewis sites. This is also supported by NH_3-TPD experiments by Chen et al., indicating that the strongest Brønsted sites are consumed in favor of a Cu-site of intermediate strength.[39] As discussed above, the number of strong Brønsted acid sites observed herein was found to be much less than, e.g., in a MOR with a similar Si/Al ratio. Given the high methanol productivity observed over Cu-MOR zeolites,[21] we conjecture that adequately strong Brønsted sites are needed to form the active Cu-oxo species for MTM. The less strong acid sites likely lead to Cu species that are either less active or inactive for methanol production. It could be that the Cu species are situated in less accessible positions like the sinusoidal 10-ring or that the Cu is positioned in the double 6-ring at the bottom of the supercages as conjectured from the FT-IR spectroscopy results. A third possibility is that the Cu is positioned on the outer surface in the half "cups" of the supercage and that there is not enough confinement or available Brønsted sites in these positions for the methoxy intermediates to stabilize on the Cu-sites. This hypothesis is supported by previous studies, revealing the half-cups to be one of the more likely sites for methylation reactions.[18]

In the third region, below −80 kJ/mol, another interesting phenomenon appears for NH_3 adsorption over Cu-loaded MCM-22. In the H-form, the sample reaches the NH_3 enthalpy of condensation at about the same amount of NH_3 adsorbed (1.4 mmol/g) as there is Al in the sample (1.1 mmol/g). However, for the Cu-exchanged samples, the adsorption continues in this low-enthalpy region for up to as much as twice the Al content, reaching an adsorption of 2.3 and 2.4 mmol/g for 0.30Cu-MCM-22 and 0.25Cu-MCM-22, respectively. If we expect some NH_3 to still be adsorbed on the remaining Brønsted sites, as observed to still be present in the Cu-sample from the OH-region of the FT-IR spectra (Figure S5), the higher amount of NH_3 adsorbed suggests that about three to four NH_3 molecules are adsorbed per Cu-site at our adsorption conditions (80 °C). This high NH_3 to Cu ratio cannot be explained by the formation of linear Cu^+ complexes ($Z[Cu(NH_3)_2]^+$) alone, and we, therefore, conjecture that a combination of this and a four-coordinated Cu^{2+} complex (e.g., $Z_2[Cu(NH_3)_4]^{2+}$) form. This is supported in a thermodynamic study over Cu-SSZ-13 by Paolucci et al., where they find that the tetraammine complex, in addition to $Z[Cu(NH_3)_2]^+$, is the most stable species ($\Delta G \approx -90$ kJ/mol) formed at 80 °C in an NH_3 atmosphere.[31] Also, other forms of the tetraammine complex could exist, where some of the NH_3 ligands are switched out with oxygen-derived species like −OH groups.[40]

In the bottom panel of Figure 5d−f, we have reported the ammonia adsorption isotherms, where the coverage of adsorbed ammonia is plotted against the pressure. Both the primary and secondary adsorption are plotted. If we first view the adsorption isotherm for H-MCM-22 (d), the shape suggests that the adsorption follows a typical Langmuir isotherm or an L-shaped isotherm based on the classification by Giles et al.[41] The secondary adsorption has the same shape, however reaching the plateau sooner, which indicates saturation at less ammonia adsorbed than for the primary. The difference between the primary and secondary adsorption isotherm gives the number of irreversible adsorption sites at 80 °C, which is an indication of the density of strong acid sites in the sample, such as Brønsted acid sites and strong Lewis acid sites. The subtracted isotherms for H-MCM-22, 0.25Cu-MCM-22, and 0.30Cu-MCM-22 are plotted in Figure S6. For the Cu-exchanged samples, the primary adsorption isotherm has a peculiar S-shape. An S-shaped isotherm is usually consistent with a scenario where there are two or more competing mechanisms at play during the adsorption.[42] For the two Cu-exchanged samples herein, we conjecture two feasible scenarios. Since NH_3 adsorbs on both H-sites and Cu-sites, and we have seen two distinct Cu-sites from CO-adsorption using FT-IR spectroscopy, the S-shape may come from varying site selectivity depending on the coverage.[42] Another scenario arrives from the above observation that NH_3 forms Cu complexes. The slow initial adsorption would then be due to the initial binding and complexation of NH_3 at the strongly adsorbing Cu-sites.[43] Then, as the level of adsorbate increases and the negative effect caused by complex formation subsides, faster adsorption is observed at higher pressures, where the Brønsted sites are also covered. Interestingly, it seems like the negative effect is no longer present for the second isotherm, and the shape is much more similar to the H-MCM-22 sample. Even so, the adsorption amount is still much higher in the Cu samples, which indicates that it is likely both the NH_3 adsorbed to Brønsted sites as well as some of the NH_3 ligands coordinated to Cu that are desorbed during outgassing. Which of the two scenarios explained is occurring would need further investigations beyond the scope of this study, although it cannot be ruled out that it is a combination of the two.

2.5. Effect of Cu on Framework Acidity. To further support our findings from NH_3-calorimetry, we also performed *n*-propylamine TPD experiments on the three samples. *n*-Propylamine can be used to solely titrate the Brønsted acid sites of a zeolite due to an acid-catalyzed Hoffmann elimination of chemisorbed *n*-propylamine that releases propene ($C_{3=}$) and NH_3. The column named "$C_{3=}$" in Table 2 gives the total amount of desorbed propene from the reaction. With the total Al in H- and Cu-MCM-22 being about

https://doi.org/10.1021/acs.iecr.3c00988
Ind. Eng. Chem. Res. 2023, 62, 10939−10950

1.0−1.1 mmol/g, and the quantity of propene observed only being 0.46−0.66 mmol/g, we surmise that a large fraction of Al in the samples has to be extra-framework Al^{3+} sites. This is also in line with our microcalorimetry results presented above. The amount of propene desorbed slightly decreases from 0.66 mmol/g for the H-MCM-22 as Cu content increases. Specifically, there is a 0.15 and 0.20 mmol/g reduction for 0.25 and 0.30Cu-MCM-22, respectively. This is consistent with Cu exchanging some of the H-sites; however, given that the Cu concentration of the two samples is 0.26 and 0.31 mmol/g, we do speculate that Cu also exchanges some strong EFAl sites like the strongly adsorbing Lewis acid sites observed in the first region of the NH_3 microcalorimetry results (Figure 5). Additionally, some propene could be confined within the zeolite framework or was subjected to undesired side reactions as we have observed to be possible over Cu-zeolites for another study in our lab and also recently reported by Lashchinskaya et al.[44]

NH_3 TPD was also employed as NH_3 can titrate both the Lewis and Brønsted acid sites in the samples and should be comparable to the results from the microcalorimetry experiment (last two columns of Table 2). The NH_3 desorption (TPD) and adsorption (microcalorimetry) values reported are in the range of 0.57−0.76 and 0.44−0.84 mmol/g, respectively. The values are a bit low considering the Al content (∼1.1 mmol/g), although in the same range and following the same trend as the values obtained from measuring the irreversible NH_3 adsorption with NH_3 calorimetry. The amount of NH_3 desorbed during the TPD experiments indicates that the total density of acid sites (Brønsted and Lewis) increases with increasing Cu content. As one Cu-site (Lewis site) would substitute either one or two Brønsted sites, there has to be something extra that contributes to the increased acid density. We surmise that the increased irreversibly adsorbed NH_3 in the Cu-zeolites compared to the H-form is coherent with Cu-sites forming Cu-ammine complexes that are strongly adsorbing, as described above. We also observe that more NH_3 is measured with NH_3 calorimetry compared to TPD. We attribute this to a higher quantity of more weakly adsorbed sites and possibly more Cu-ammine complexes remaining after outgassing at 80 °C (between the primary and secondary adsorption), compared to the amount remaining after flushing at 170 °C in He before the TPD experiment.

Lastly, it is also of interest to point out the peak desorption temperatures during the NH_3-TPD experiments. As reported in Figure 6, the H-MCM-22 sample has a broad peak (maximum at 350 °C) assigned to Brønsted acid sites. Note that the broad nature of the peak is in line with the heterogeneity of acid site strengths first observed with NH_3 calorimetry on the H-form. The two Cu-exchanged samples, however, have three major peaks, specifically at 275, 350, and 450 °C. This is similar to what has been observed on a set of Cu-loaded MCM-22 materials previously by Chen et al.[39] The peak at 350 °C reduces with increasing Cu-loading, supporting that this desorption temperature is linked with Brønsted acid sites. Based on the above discussion, we infer that the other two peaks come from NH_3 molecules being desorbed from the $Z[Cu(NH_3)_2]^+$ and $Z_2[Cu(NH_3)_4]^{2+}$ complexes residing after adsorption. According to the phase diagram reported by Paolucci et al. on Cu-SSZ-13,[31] and in situ XAS TPD experiments by Borfecchia et al.,[40] we surmise that the low-temperature peak is from NH_3 desorbing from tetraammine-derived complexes. This peak is stronger in the 0.30Cu-MCM-22, which indicates that a higher concentration of Cu leads to more sites available for tetraammine complexation. As this requires more space, we could presume that this site is more easily accessible than the site forming diammine complexes; however, it should be kept in mind that the diammine complex forms on reduced Cu-sites, so it is plausible that it is rather reducibility and not accessibility that governs the amount of diammine and tetraammine complexes. The broad high-temperature peak is likely to come from Cu-sites with different strengths, however stronger than Brønsted acid sites. This correlates well with species desorbing from both the diamine and tetraammine complexes.[31]

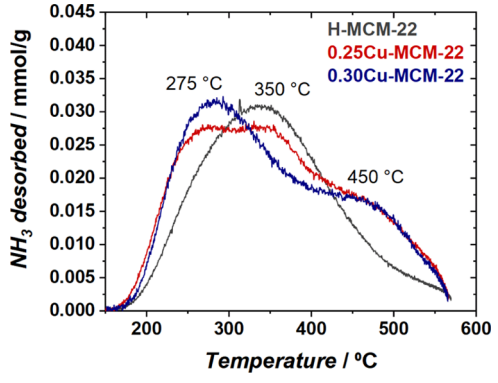

Figure 6. NH_3-TPD profiles of H-MCM-22, 0.25Cu-MCM-22, and 0.30Cu-MCM-22.

2.6. Preliminary Microcalorimetry Experiments with CH_4. Thus far, the results reported herein indicate that Cu introduces some stronger adsorption sites to the zeolite, and we could hypothesize that it is the effect of these in addition to the redox capability that leads to selective methanol production from methane. As an additional experiment to broaden the scope of microcalorimetry experiments and obtain results that were directly applicable to the MTM reaction, we attempted microcalorimetry experiments with CH_4 at 300 °C to be close to the temperatures for methane activation in the MTM reaction. The results obtained for 0.30Cu-MCM-22 are reported in Figure 7, where (a) gives the adsorption isotherm, and (b) gives the corresponding heat of adsorption measured. The adsorption isotherm appears to be a straight line up to as much as 80 mbar of CH_4, with no apparent adsorption or effect from the partitioning of CH_4 when interacting with the zeolite confinement. Additionally, as observed in Figure 7b, where the adsorption heat appears close to −5 kJ/mol for the entire adsorption experiment, there are no signs of CH_4 oxidation on the Cu-sites. In an earlier CH_4 microcalorimetry experiment by Yang et al.,[45] it was shown that the differential heat for CH_4 adsorption lay around 28−14 kJ/mol, depending on the H-zeolite. The values were constant with coverage, similar to what we observe herein. However, they observed slightly stronger heats of adsorption, possibly due to the lower temperature of their experiments (−63.15 °C), which was done to obtain close to complete filling of the pores and cavities, leading to stronger interactions. The CH_4 adsorption experiment reported here gives a picture of how weak the adsorption interaction of CH_4 is with Cu-zeolites at the temperature of CH_4 exposure in MTM and could perhaps explain why only some types of Cu_xO_y-moieties can activate CH_4 in zeolites.[46] The results also indicate why it is easier to

https://doi.org/10.1021/acs.iecr.3c00988
Ind. Eng. Chem. Res. 2023, 62, 10939−10950

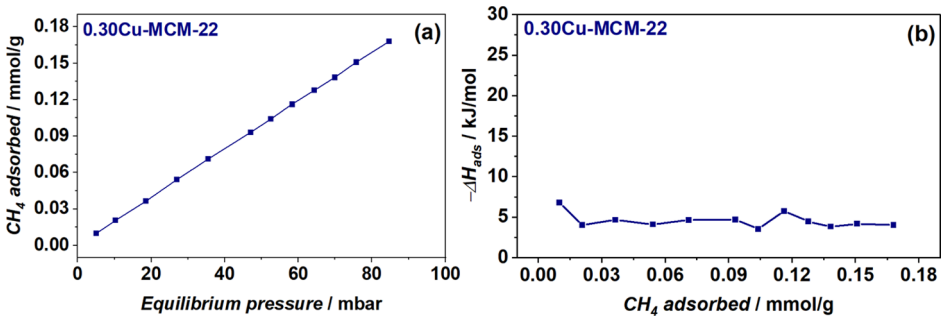

Figure 7. Differential heats of adsorption (a) and adsorption isotherm (b) for CH_4 over 0.30Cu-MCM-22. The adsorption isotherm is given as adsorbed CH_4 in μmol/g per equilibrium pressure (mbar). Differential heats of adsorption (kJ/mol) are plotted against the CH_4 adsorbed in μmol/g.

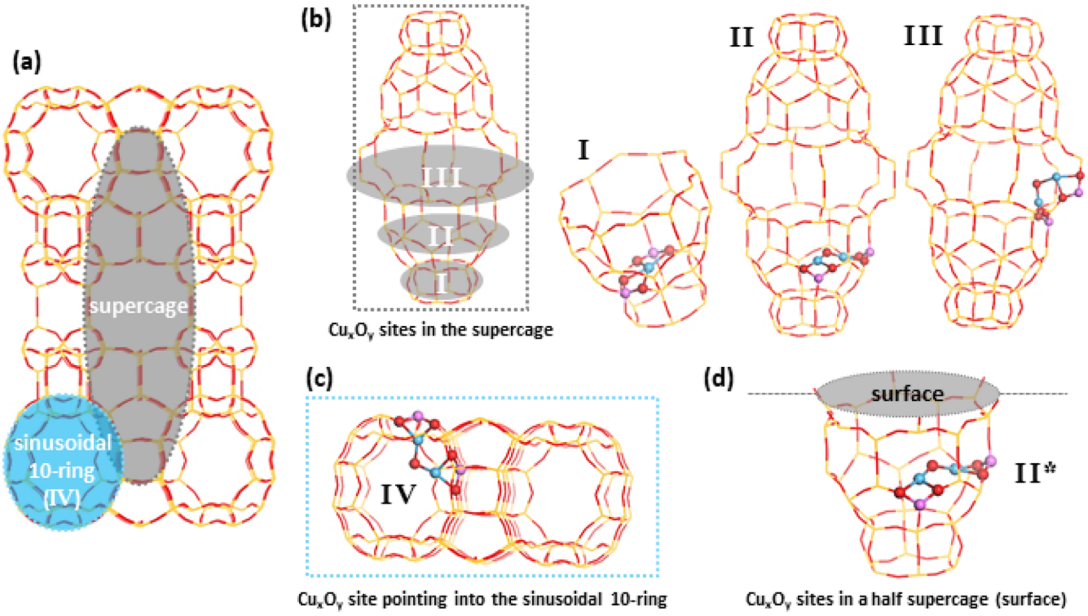

Figure 8. Representation of likely Cu_xO_y-site positions in the MCM-22 channels. (a) Provides an overview of the two individual channels present in the material, both accessible from 10-ring openings. (b) Shows three possible positions for Cu_xO_y-sites within the supercage. I shows a four-coordinated site situated in the double 6-ring, while II and III are situated at possible T-sites in the supercage cavity. (c) represents a likely position (IV) within the sinusoidal 10-ring, and (d) shows how the supercage is opened up, exposing Cu-sites (e.g., II*) on the external surface of the material.

utilize more Cu_xO_y-sites with a higher methane loading pressure (8−37 bar), as previously reported.[7,12,47−49]

3. CU-SITE FORMATION IN MCM-22

To summarize the findings, we will in this section explain the results in view of likely positions for Cu to be situated in MCM-22. A representation of both channel systems within MCM-22 is given in Figure 8a, namely, the sinusoidal 10-ring as well as the supercage accessible through 10-rings. The Cu-sites given in Figure 8b−d are based on the position of possible T-sites .[50] Three anchoring sites (I, II, and III) are illustrated for the supercage, while a fourth option is that the Cu-sites point into the sinusoidal 10-ring. Lastly, it should be mentioned that the Cu-sites in the supercage could be less confined when they are positioned in half-cups that point toward the external surface (e.g., position II* represented in Figure 8d). From FT-IR spectroscopy, we learned that there are at least two spectroscopically different Cu-sites in MCM-22. Frolich et al. linked the two bands with Cu in the center of the supercage (position II or III) and possibly Cu in the double 6-ring (position I).[30] In the double 6-rings of Cu-CHA zeolites, Cu species coordinated to both one (1Al) and two (2Al) framework Al are proposed to exist.[31] In the FT-IR spectroscopy results herein, however, only 1Al coordinated Cu species would be traceable with CO-adsorption as the 2Al coordinated Cu-sites are redox inactive in vacuum. With that being said, if Cu^+ species are observed in the double 6-ring as proposed by Frolich et al., it is not unlikely that some of the double 6-rings in MCM-22 also contain 2Al that forms redox inert Cu^{2+} sites as well, which would be unreactive for MTM conversion. The existence of such redox inactive sites could play a partial role in the moderate C−H activation capacity observed for MCM-22.

When testing the 2D materials, ITQ-2 and MCM-36, we showed that the surface pockets (site II*) and the sinusoidal channel (site IV), which are the only sites remaining in the 2D materials, are less active and less selective in MTM. This suggests that the most productive sites likely lie in the supercage. As some of the sites in the double 6-ring (at the bottom of the supercage) could be Cu coordinated to 2Al and

https://doi.org/10.1021/acs.iecr.3c00988
Ind. Eng. Chem. Res. 2023, 62, 10939−10950

thus be inactive (site I), by process of elimination, this suggests that site II, III, or 1Al Cu-sites in position I (e.g., Cu−OH) are likely the most active for methane to methanol.

Furthermore, with this study, we have shown the broad nature of acid sites in MCM-22 with the help of NH_3-calorimetry as well as *n*-propylamine and NH_3-TPD, which likely explains why the MCM-22 tested herein has been less active for MTM, compared to other zeolite frameworks. The adsorption/desorption results suggest that there are only a small fraction of strongly adsorbing Brønsted and Lewis sites, while the other acid sites are weaker and inhomogeneous. This inhomogeneity even of the Brønsted sites indicates that Brønsted sites are found in several different sites, which is supported by the large number of T-sites within the framework. From the NH_3 calorimetry results on H-MCM-22, we find that only 30% of the acid sites have an acid site strength above ΔH_{ads} = 90 kJ/mol. Weaker Brønsted acid strength is often connected with lower reactivity in acid-catalyzed reactions[51] and could likely influence both the speciation and activity of Cu-sites that form on these sites. In a paper, Katada et al. show that Brønsted acid sites in more open confinements like position III and II* in MCM-22 are weaker than more confined spaces like in the sinusoidal 10-ring and the bottom of the supercage.[52] In a work by Chen et al.,[53] they deconvolute the desorption peak for NH_3 on H-MCM-22 and assign it to strong and weak acid sites, identifying about 46% weak acid sites. With Py-IR, they are able to separate between acid sites in the sinusoidal 10-ring (33%), the supercage (52%), and the external half-supercage pockets (15%). As much as 38% of the total acid sites are also found to be Lewis acid sites, rather than Brønsted acid sites using Py-IR, and these sites are mostly situated in the supercage. These large numbers of weak acid sites and Lewis acid sites fit well with our findings. Additionally, they find with NMR that as much as 16% of the total Al content is present as EFAl, also supporting our findings of a large fraction of EFAl in MCM-22.

Taken together, the results by Chen et al. support the indication that, in our materials, we likely have a large fraction of acid sites in the supercage and the surface pockets which presents several different possible sites for the resulting Cu-oxo species, as shown in Figure 8.[53] Due to the very open confinement around position III, we propose site II or 1Al Cu-sites in position I (e.g., Cu−OH) to be the most likely positions to form active Cu-sites for MTM. Combined with the significant fraction of weak acid sites, we question whether a sufficiently large concentration of idealized Cu-oxo host sites (i.e., acid sites of adequate strength) are present within the MCM-22 framework for MTM conversion.

4. CONCLUSIONS

This study investigated Cu-loaded MCM-22 as a hitherto unexplored material for the MTM reaction. The results suggested that the material was, indeed, able to form methanol from methane. To understand the impact of this unexplored zeolite structure on methanol productivity, a deeper study of the material properties was executed. With the help of methods like SEM imaging, PXRD, and XAS on O_2-activated samples, we showed that the Cu-zeolites had no discernible nanoparticles and that the Cu ions were well distributed and redox-active. This suggested that the more moderate activity toward methanol compared to other zeolite systems was not a result of improper zeolite synthesis or ion exchange. It rather had to be connected with the Cu-speciation, and we, therefore, needed to study the possible implications from the framework topology on the Cu-speciation. To that end, CO-adsorption coupled with FT-IR spectroscopy, NH_3-calorimetry, and *n*-propylamine- and NH_3-TPD experiments were applied as these were methods that gave comparable information about the cationic sites. We show that there are few homogeneously strong Brønsted acid sites in MCM-22 before Cu exchange and that these strong Brønsted sites are likely the sites leading to a Cu-oxo speciation available for C−H activation. CO-adsorption with FT-IR also reveals that there are at least two distinctly different ion exchange sites for Cu. Combined, we hypothesize that the complex structure of MCM-22 led to few sites where all the requirements needed for selective C−H activation were present. Among the Cu-sites formed, a significant concentration was either inactive, inaccessible to methane, or unable to stabilize reaction intermediates. Furthermore, as a preliminary study, a CH_4-calorimetry experiment also revealed that CH_4 interaction is very weak (low heat of adsorption), unraveling some of the reasons behind why specific Cu_xO_y-sites are needed to activate CH_4. This study has shown that adequately strong acid sites before Cu exchange are important to form the active sites for methane activation to methanol. For MCM-22, the lack of such sites is connected with the zeolite topology and forms an additional contribution toward the search for optimal structures in the MTM reaction and for other C−H activation reactions.

5. EXPERIMENTAL DETAILS

5.1. Performance Measurements. All MTM tests were performed on a purpose-designed setup previously used for the MTM reaction.[9,11,21,28] 100 mg of sample was weighed, sieved (425−250 μm), and placed in a linear quartz tube reactor (i.d. = 6 mm). A thermocouple inside the oven was used to control the temperature. The temperature set points were calibrated prior to the experiments by placing a thermocouple inside a quartz sheet touching a reactor bed while following a full protocol. A stepwise protocol was applied for the experiments. The gases were kept separate with the help of different MFCs for each gas, stop-, and 4-way valves. The following protocol was applied: the sample was first activated in O_2 (100%) at 500 °C (8 h). Then, the temperature was lowered (5 °C/min) to 200 °C, and He (100%) was sent onto the sample (45 min) to flush the system. Then, CH_4 (100%) was sent onto the sample (3 h) before a second flushing step in He (45 min) was initiated. Finally, a Ne/He (10%/rest) flow saturated with 10% water was sent onto the sample (2 h). All gas flows were set to 15 mL/min. An online quadrupole mass spectrometer (Omnistar GSD320, Pfeiffer) was connected to the outlet of the reactor to analyze the effluent. The quantitative analysis of the products [MeOH (m/z = 31), DME (m/z = 46), and CO_2 (m/z = 44)] in μmol/g was obtained with the help of an external calibration bottle with known amounts of the products. The methanol yield is reported herein as MeOH + 2xDME.

5.2. X-ray Absorption Spectroscopy. XAS experiments were performed at RT on presealed capillaries (i.d. = 1.5 mm, thickness = 0.1 μm) at the Balder beamline at MAX IV in Lund, Sweden. The samples were pretreated in open capillaries at 500 °C in air overnight and sealed at high temperature before being cooled to RT. A Si(111) double-crystal monochromator was employed, and the monochromator was calibrated against a premeasured Cu-foil. Cu K-edge spectra of the Cu-exchanged materials were collected in transmission

https://doi.org/10.1021/acs.iecr.3c00988
Ind. Eng. Chem. Res. 2023, 62, 10939−10950

mode, and ionization chambers were used for detection. The EXAFS scans were acquired in the 8795−9730 eV range, with an acquisition time of 3 min/scan. Six scans were accumulated and merged by averaging the $\mu(E)$ curves during analysis for better quality. Two XANES scans per sample were acquired separately in the 8815−9175 eV range, with an acquisition time of 45 s/scan. The XANES scans were also merged for better data quality. For analysis, all XAS spectra were normalized to unity edge jump and afterward aligned in energy with the help of Athena software from the Demeter package.[54] By using the Athena program, the $\chi(k)$ and EXAFS functions were extracted, and the Fourier-transform (FT) EXAFS spectra were obtained by transforming the k^2 $\chi(k)$ functions in the range of 2.4−10.0 $Å^{-1}$.

5.3. CO-Adsorption Coupled with FT-IR Spectroscopy. CO-adsorption experiments on the Cu-exchanged samples were performed at RT and measured on a Bruker Vertex 70 instrument, equipped with a Mercury−Cadmium−Telluride (MCT) detector. A thin, self-supporting wafer (∼10 mg/cm^2) of each sample was prepared and fitted inside a gold envelope. The envelope was placed in a low-temperature vacuum cell with KBr windows before being ramped up (5 °C/min) to 450 °C and kept for 1.5 h. After being cooled to RT, incremental amounts of CO were dosed onto the sample, while an IR spectrum was collected after every dose, until reaching the equilibrium pressure of about 8 mbar.

5.4. Adsorption Microcalorimetry (NH_3- and CH_4-Adsorption). The adsorption of ammonia was carried out in a stepwise fashion. Small doses of ammonia were introduced to the sample placed in a quartz calorimetric cell maintained at 80 °C. The adsorption microcalorimetry setup comprised a manometric adsorption apparatus (with a dynamic vacuum of 10^{-5} mbar) coupled with a Tian-Calvet-type heat flow calorimeter (Setaram C80, sensitivity 0.1 μW resolution). The setup measures the adsorption isotherms and enthalpies of adsorption simultaneously using stepwise introduction of the gas to the sample. A capacitance manometer (MKS Baratron 670A, range 0−10 Torr) was used to achieve pressure measurements. The heat flow signal observed upon introduction of gas to the sample was allowed to return to the baseline before introduction of the subsequent dose. Integration of the heat flow signal was performed using Calisto v1.066 AKTS-Setaram software.

Prior to each adsorption experiment, the samples were pretreated and activated following the following protocol. Typically, 0.2−0.3 g of sample was placed in the calorimetric cell. The sample was dried in argon at 160 °C for 1−3 h, followed by a temperature ramp in pure oxygen at 5 °C min^{-1} to 500 °C. The sample was held at 500 °C for 480 min before cooling to 200 °C in oxygen flow. Once at 200 °C, the flow was switched back to argon for 60 min and later cooled to room temperature and isolated from the external atmosphere to avoid exposing the activated sample to atmospheric humidity. The sample containing the cell was transferred to the calorimeter, well maintained at 80 °C, and outgassed to a dynamic vacuum of 10^{-8} mbar until a stable baseline was achieved. Successive micromolar doses of NH_3 were introduced to the sample until the sample became saturated (i.e., no noticeable changes in the heat flow signal with more doses). Between the primary and secondary adsorption, the sample was outgassed at 80 °C for ∼10 h until the heat flow curve returned to the baseline.

The same protocol was followed for CH_4 adsorption, except that the adsorption temperature was set to 300 °C.

5.5. TPD Experiments. *n*-Propylamine-TPD experiments to study the amount of Brønsted acid sites of both the protonic and Cu-exchanged material were performed on a homemade flow setup. The effluent from the desorption was detected by an online Pfeiffer Omnistar quadrupole mass spectrometer. About 30 mg of the sample was activated in a flow of synthetic air (50 mL/min) for 1 h at 500 °C (ramp rate = 10 °C/min). The sample was then cooled to 170 °C before being exposed to N_2 gas flow (50 mL/min) saturated with *n*-propylamine vapors for 1 h. All excess *n*-propylamine was flushed from the system with N_2 (66 mL/min, 4 h) before the desorption protocol was initiated (ramping 10 °C/min in 66 mL/min N_2 up to 500 °C). The total amount of propene (m/z = 41) released from the system was quantified using a calibration gas that was sent into the system at the end of the experiment.

NH_3-TPD was performed on ca. 30 mg of pelletized protonic and Cu-exchanged zeolites in a comparable manner to the *n*-propylamine-TPD. After an initial activation step in synthetic air, the sample kept at 170 °C was exposed to 2% NH_3 in N_2 (50 mL/min) for 4 h. This was followed by flushing in inert N_2 (66 mL/min) for 4 h before heating to 575 °C (10 °C/min) in N_2. The amount of NH_3 released (m/z = 16) was quantified using the calibrant 2% NH_3 in N_2 upon stabilizing at the end of the adsorption step.

■ ASSOCIATED CONTENT

Supporting Information

The Supporting Information is available free of charge at https://pubs.acs.org/doi/10.1021/acs.iecr.3c00988.

Experimental methods (material preparation and standard characterization), physicochemical data (PXRD, N_2-physisorption, TGA), details on XAS spectral features, additional FT-IR spectra, and subtracted isotherms (PDF)

■ AUTHOR INFORMATION

Corresponding Author

Stian Svelle − *Center for Materials Science and Nanotechnology, Department of Chemistry, University of Oslo, 0315 Oslo, Norway;* orcid.org/0000-0002-7468-5546; Email: stian.svelle@kjemi.uio.no

Authors

Karoline Kvande − *Center for Materials Science and Nanotechnology, Department of Chemistry, University of Oslo, 0315 Oslo, Norway;* orcid.org/0000-0002-0154-0346

Moses Mawanga − *Department of Chemical Engineering, Norwegian University of Science and Technology (NTNU), NO-7491 Trondheim, Norway*

Sebastian Prodinger − *Center for Materials Science and Nanotechnology, Department of Chemistry, University of Oslo, 0315 Oslo, Norway;* orcid.org/0000-0001-8749-0476

Bjørn Gading Solemsli − *Center for Materials Science and Nanotechnology, Department of Chemistry, University of Oslo, 0315 Oslo, Norway*

Jia Yang − *Department of Chemical Engineering, Norwegian University of Science and Technology (NTNU), NO-7491 Trondheim, Norway*

Unni Olsbye − *Center for Materials Science and Nanotechnology, Department of Chemistry, University of Oslo, 0315 Oslo, Norway;* orcid.org/0000-0003-3693-2857

Pablo Beato − *Topsoe A/S, DK-2800 Kgs. Lyngby, Denmark*

Edd Anders Blekkan − *Department of Chemical Engineering, Norwegian University of Science and Technology (NTNU), NO-7491 Trondheim, Norway;* orcid.org/0000-0002-3620-3884

Complete contact information is available at: https://pubs.acs.org/10.1021/acs.iecr.3c00988

Notes

The authors declare no competing financial interest.

■ ACKNOWLEDGMENTS

This publication forms a part of the iCSI (industrial Catalysis Science and Innovation) Centre for Research-based Innovation, which receives financial support from the Research Council of Norway under contract no. 237922. M. Sørensen is acknowledged for his work synthesizing the as-made MCM-22. E. Borfecchia is acknowledged for her valuable insight and support in interpreting the XAS results. We acknowledge MAX IV Laboratory for time on Beamline Balder under Proposal 20190347. Research conducted at MAX IV, a Swedish national user facility, is supported by the Swedish Research Council under contract 2018-07152, the Swedish Governmental Agency for Innovation Systems under contract 2018-04969, and Formas under contract 2019-02496. The staff at Balder, M. Ciambezi, J. Just, and K. Klementiev, is acknowledged for their help and support during our experiment. TOC is created with Biorender.com.

■ REFERENCES

(1) Lunsford, J. H. Catalytic conversion of methane to more useful chemicals and fuels: a challenge for the 21st century. *Catal. Today* **2000**, *63*, 165−174.

(2) Groothaert, M. H.; Smeets, P. J.; Sels, B. F.; Jacobs, P. A.; Schoonheydt, R. A. Selective oxidation of methane by the bis(μ-oxo)dicopper core stabilized on ZSM-5 and mordenite zeolites. *J. Am. Chem. Soc.* **2005**, *127*, 1394−1395.

(3) Sushkevich, V. L.; Palagin, D.; Ranocchiari, M.; van Bokhoven, J. A. Selective Anaerobic Oxidation of Methane Enables Direct Synthesis of Methanol. *Science* **2017**, *356*, 523−527.

(4) Alayon, E. M.; Nachtegaal, M.; Ranocchiari, M.; van Bokhoven, J. A. Catalytic conversion of methane to methanol over Cu-mordenite. *Chem. Commun.* **2012**, *48*, 404−406.

(5) Grundner, S.; Markovits, M. A.; Li, G.; Tromp, M.; Pidko, E. A.; Hensen, E. J.; Jentys, A.; Sanchez-Sanchez, M.; Lercher, J. A. Single-site trinuclear copper oxygen clusters in mordenite for selective conversion of methane to methanol. *Nat. Commun.* **2015**, *6*, 7546.

(6) Grundner, S.; Luo, W.; Sanchez-Sanchez, M.; Lercher, J. A. Synthesis of Single-Site Copper Catalysts for Methane Partial Oxidation. *Chem. Commun.* **2016**, *52*, 2553−2556.

(7) Tomkins, P.; Mansouri, A.; Bozbag, S. E.; Krumeich, F.; Park, M. B.; Alayon, E. M.; Ranocchiari, M.; van Bokhoven, J. A. Isothermal Cyclic Conversion of Methane into Methanol over Copper-Exchanged Zeolite at Low Temperature. *Angew. Chem., Int. Ed.* **2016**, *55*, 5467−5471.

(8) Prodinger, S.; Kvande, K.; Arstad, B.; Borfecchia, E.; Beato, P.; Svelle, S. Synthesis−Structure−Activity Relationship in Cu-MOR for Partial Methane Oxidation: Al Siting via Inorganic Structure-Directing Agents. *ACS Catal.* **2022**, *12*, 2166−2177.

(9) Pappas, D. K.; Borfecchia, E.; Dyballa, M.; Pankin, I. A.; Lomachenko, K. A.; Martini, A.; Signorile, M.; Teketel, S.; Arstad, B.; Berlier, G.; Lamberti, C.; Bordiga, S.; Olsbye, U.; Lillerud, K. P.; Svelle, S.; Beato, P. Methane to Methanol: Structure-Activity Relationships for Cu-CHA. *J. Am. Chem. Soc.* **2017**, *139*, 14961−14975.

(10) Wulfers, M. J.; Teketel, S.; Ipek, B.; Lobo, R. F. Conversion of methane to methanol on copper-containing small-pore zeolites and zeotypes. *Chem. Commun.* **2015**, *51*, 4447−4450.

(11) Pappas, D. K.; Borfecchia, E.; Dyballa, M.; Lomachenko, K. A.; Martini, A.; Berlier, G.; Arstad, B.; Lamberti, C.; Bordiga, S.; Olsbye, U.; Svelle, S.; Beato, P. Understanding and Optimizing the Performance of Cu-FER for The Direct CH_4 to CH_3OH Conversion. *ChemCatChem* **2019**, *11*, 621−627.

(12) Sushkevich, V. L.; van Bokhoven, J. A. Methane-to-Methanol: Activity Descriptors in Copper-Exchanged Zeolites for the Rational Design of Materials. *ACS Catal.* **2019**, *9*, 6293−6304.

(13) Knorpp, A. J.; Pinar, A. B.; Newton, M. A.; Sushkevich, V. L.; van Bokhoven, J. A. Copper-Exchanged Omega (MAZ) Zeolite: Copper-Concentration Dependent Active Sites and its Unprecedented Methane to Methanol Conversion. *ChemCatChem* **2018**, *10*, 5593−5596.

(14) Ravishankar, R.; Bhattacharya, D.; Jacob, N. E.; Sivasanker, S. Characterization and catalytic properties of zeolite MCM-22. *Microporous Mater.* **1995**, *4*, 83−93.

(15) Bjørgen, M.; Akyalcin, S.; Olsbye, U.; Benard, S.; Kolboe, S.; Svelle, S. Methanol to hydrocarbons over large cavity zeolites: Toward a unified description of catalyst deactivation and the reaction mechanism. *J. Catal.* **2010**, *275*, 170−180.

(16) Leonowicz, M. E.; Lawton, J. A.; Lawton, S. L.; Rubin, M. K. MCM-22: A Molecular Sieve with Two Independent Multidimensional Channel Systems. *Science* **1994**, *264*, 1910−1913.

(17) Souverijns, W.; Verrelst, W.; Vanbutsele, G.; Martens, J. A.; Jacobs, P. A. Micropore structure of zeolite MCM-22 as determined by the decane catalytic test reaction. *J. Chem. Soc., Chem. Commun.* **1994**, 1671−1672.

(18) Lawton, S. L.; Leonowicz, M. E.; Partridge, R. D.; Chu, P.; Rubin, M. K. Twelve-ring pockets on the external surface of MCM-22 crystals. *Microporous Mesoporous Mater.* **1998**, *23*, 109−117.

(19) Corma, A.; Corell, C.; Pérez-Pariente, J. Synthesis and characterization of the MCM-22 zeolite. *Zeolites* **1995**, *15*, 2−8.

(20) Dyballa, M.; Pappas, D. K.; Kvande, K.; Borfecchia, E.; Arstad, B.; Beato, P.; Olsbye, U.; Svelle, S. On How Copper Mordenite Properties Govern the Framework Stability and Activity in the Methane-to-Methanol Conversion. *ACS Catal.* **2019**, *9*, 365−375.

(21) Pappas, D. K.; Martini, A.; Dyballa, M.; Kvande, K.; Teketel, S.; Lomachenko, K. A.; Baran, R.; Glatzel, P.; Arstad, B.; Berlier, G.; Lamberti, C.; Bordiga, S.; Olsbye, U.; Svelle, S.; Beato, P.; Borfecchia, E. The Nuclearity of the Active Site for Methane to Methanol Conversion in Cu-Mordenite: A Quantitative Assessment. *J. Am. Chem. Soc.* **2018**, *140*, 15270−15278.

(22) Min, H.-K.; Park, M. B.; Hong, S. B. Methanol-to-olefin conversion over H-MCM-22 and H-ITQ-2 zeolites. *J. Catal.* **2010**, *271*, 186−194.

(23) Svelle, S.; Visur, M.; Olsbye, U.; Saepurahman; Bjørgen, M. Mechanistic Aspects of the Zeolite Catalyzed Methylation of Alkenes and Aromatics with Methanol: A Review. *Top. Catal.* **2011**, *54*, 897.

(24) Wang, S.; Wei, Z.; Chen, Y.; Qin, Z.; Ma, H.; Dong, M.; Fan, W.; Wang, J. Methanol to Olefins over H-MCM-22 Zeolite: Theoretical Study on the Catalytic Roles of Various Pores. *ACS Catal.* **2015**, *5*, 1131−1144.

(25) Borfecchia, E.; Lomachenko, K. A.; Giordanino, F.; Falsig, H.; Beato, P.; Soldatov, A. V.; Bordiga, S.; Lamberti, C. Revisiting the Nature of Cu sites in the Activated Cu-SSZ-13 Catalyst for SCR reaction. *Chem. Sci.* **2015**, *6*, 548−563.

(26) Llabrés i Xamena, F. X.; Fisicaro, P.; Berlier, G.; Zecchina, A.; Palomino, G. T.; Prestipino, C.; Bordiga, S.; Giamello, E.; Lamberti, C. Thermal Reduction of Cu^{2+}−Mordenite and Re-oxidation upon Interaction with H_2O, O_2, and NO. *J. Phys. Chem. B* **2003**, *107*, 7036−7044.

(27) Pappas, D. K.; Kvande, K.; Kalyva, M.; Dyballa, M.; Lomachenko, K. A.; Arstad, B.; Borfecchia, E.; Bordiga, S.; Olsbye, U.; Beato, P.; Svelle, S. Influence of Cu-speciation in mordenite on direct methane to methanol conversion: Multi-Technique characterization and comparison with NH3 selective catalytic reduction of NOx. *Catal. Today* **2021**, *369*, 105−111.
(28) Kvande, K.; Pappas, D. K.; Dyballa, M.; Buono, C.; Signorile, M.; Borfecchia, E.; Lomachenko, K. A.; Arstad, B.; Bordiga, S.; Berlier, G.; Olsbye, U.; Beato, P.; Svelle, S. Comparing the Nature of Active Sites in Cu-loaded SAPO-34 and SSZ-13 for the Direct Conversion of Methane to Methanol. *Catalysts* **2020**, *10*, 191.
(29) Giordanino, F.; Vennestrom, P. N. R.; Lundegaard, L. F.; Stappen, F. N.; Mossin, S.; Beato, P.; Bordiga, S.; Lamberti, C. Characterization of Cu-Exchanged SSZ-13: a Comparative FTIR, UV-Vis, and EPR Study with Cu-ZSM-5 and Cu-beta with Similar Si/Al and Cu/Al Ratios. *Dalton Trans.* **2013**, *42*, 12741−12761.
(30) Frolich, K.; Bulánek, R.; Frýdová, E. Interaction of CO probe molecules with Cu(+) in MCM-22 zeolite. *Microporous Mesoporous Mater.* **2014**, *186*, 37−45.
(31) Paolucci, C.; Parekh, A. A.; Khurana, I.; Di Iorio, J. R.; Li, H.; Albarracin Caballero, J. D.; Shih, A. J.; Anggara, T.; Delgass, W. N.; Miller, J. T.; Ribeiro, F. H.; Gounder, R.; Schneider, W. F. Catalysis in a Cage: Condition-Dependent Speciation and Dynamics of Exchanged Cu Cations in SSZ-13 Zeolites. *J. Am. Chem. Soc.* **2016**, *138*, 6028−6048.
(32) Kustov, L. M.; Kazanskii, V. B.; Beran, S.; Kubelkova, L.; Jiru, P. Adsorption of carbon monoxide on ZSM-5 zeolites: infrared spectroscopic study and quantum-chemical calculations. *J. Phys. Chem.* **1987**, *91*, 5247−5251.
(33) Bordiga, S.; Lamberti, C.; Bonino, F.; Travert, A.; Thibault-Starzyk, F. Probing zeolites by vibrational spectroscopies. *Chem. Soc. Rev.* **2015**, *44*, 7262−7341.
(34) Auroux, A. Acidity and basicity: determination by adsorption microcalorimetry. In *Acidity and Basicity*; Karge, H. G., Weitkamp, J., Eds.; *Molecular Sieves*; Springer-Verlag: Berlin Heidelberg, 2006; Vol. 6, pp 45−152.
(35) Parrillo, D. J.; Gorte, R. J. Characterization of acidity in H-ZSM-5, H-ZSM-12, H-Mordenite, and H-Y using microcalorimetry. *J. Phys. Chem.* **1993**, *97*, 8786−8792.
(36) Busca, G.; Lietti, L.; Ramis, G.; Berti, F. Chemical and mechanistic aspects of the selective catalytic reduction of NO by ammonia over oxide catalysts: A review. *Appl. Catal., B* **1998**, *18*, 1−36.
(37) Arrigo, R.; Wrabetz, S.; Schuster, M. E.; Wang, D.; Villa, A.; Rosenthal, D.; Girsgdies, F.; Weinberg, G.; Prati, L.; Schlögl, R.; Su, D. S. Tailoring the morphology of Pd nanoparticles on CNTs by nitrogen and oxygen functionalization. *Phys. Chem. Chem. Phys.* **2012**, *14*, 10523−10532.
(38) Giordanino, F.; Borfecchia, E.; Lomachenko, K. A.; Lazzarini, A.; Agostini, G.; Gallo, E.; Soldatov, A. V.; Beato, P.; Bordiga, S.; Lamberti, C. Interaction of NH_3 with Cu-SSZ-13 Catalyst: A Complementary FTIR, XANES, and XES Study. *J. Phys. Chem. Lett.* **2014**, *5*, 1552−1559.
(39) Chen, J.; Peng, G.; Liang, T.; Zhang, W.; Zheng, W.; Zhao, H.; Guo, L.; Wu, X. Catalytic Performances of Cu/MCM-22 Zeolites with Different Cu Loadings in NH3-SCR. *Nanomaterials* **2020**, *10*, 2170.
(40) Borfecchia, E.; Negri, C.; Lomachenko, K. A.; Lamberti, C.; Janssens, T. V. W.; Berlier, G. Temperature-dependent dynamics of NH3-derived Cu species in the Cu-CHA SCR catalyst. *React. Chem. Eng.* **2019**, *4*, 1067−1080.
(41) Giles, C. H.; Smith, D.; Huitson, A. A general treatment and classification of the solute adsorption isotherm. I. Theoretical. *J. Colloid Interface Sci.* **1974**, *47*, 755−765.
(42) Inglezakis, V. J.; Poulopoulos, S. G.; Kazemian, H. Insights into the S-shaped sorption isotherms and their dimensionless forms. *Microporous Mesoporous Mater.* **2018**, *272*, 166−176.
(43) Limousin, G.; Gaudet, J. P.; Charlet, L.; Szenknect, S.; Barthès, V.; Krimissa, M. Sorption isotherms: A review on physical bases, modeling and measurement. *Appl. Geochem.* **2007**, *22*, 249−275.
(44) Lashchinskaya, Z. N.; Gabrienko, A. A.; Stepanov, A. G. Propene transformation on Cu-modified ZSM-5 zeolite: Aromatization and oxidation. *Microporous Mesoporous Mater.* **2023**, *350*, 112448.
(45) Yang, L.; Trafford, K.; Kresnawahjuesa, O.; Šepa, J.; Gorte, R. J.; White, D. An Examination of Confinement Effects in High-Silica Zeolites. *J. Phys. Chem. B* **2001**, *105*, 1935−1942.
(46) Park, M. B.; Park, E. D.; Ahn, W.-S. Recent Progress in Direct Conversion of Methane to Methanol Over Copper-Exchanged Zeolites. *Front. Chem.* **2019**, *7*, 514.
(47) Tomkins, P.; Ranocchiari, M.; van Bokhoven, J. A. Direct Conversion of Methane to Methanol under Mild Conditions over Cu-Zeolites and Beyond. *Acc. Chem. Res.* **2017**, *50*, 418−425.
(48) Brezicki, G.; Kammert, J. D.; Gunnoe, T. B.; Paolucci, C.; Davis, R. J. Insights into the Speciation of Cu in the Cu-H-Mordenite Catalyst for the Oxidation of Methane to Methanol. *ACS Catal.* **2019**, *9*, 5308−5319.
(49) Zheng, J.; Lee, I.; Khramenkova, E.; Wang, M.; Peng, B.; Gutierrez, O. Y.; Fulton, J. L.; Camaioni, D. M.; Khare, R.; Jentys, A.; Haller, G. L.; Pidko, E. A.; Sanchez-Sanchez, M.; Lercher, J. A. Importance of Methane Chemical Potential for Its Conversion to Methanol on Cu-Exchanged Mordenite. *Chem.—Eur. J.* **2020**, *26*, 7563−7567.
(50) Schwanke, A.; Pergher, S. Lamellar MWW-Type Zeolites: Toward Elegant Nanoporous Materials. *Appl. Sci.* **2018**, *8*, 1636.
(51) Liu, C.; Tranca, I.; van Santen, R. A.; Hensen, E. J. M.; Pidko, E. A. Scaling Relations for Acidity and Reactivity of Zeolites. *J. Phys. Chem. C* **2017**, *121*, 23520−23530.
(52) Katada, N.; Suzuki, K.; Noda, T.; Sastre, G.; Niwa, M. Correlation between Brønsted Acid Strength and Local Structure in Zeolites. *J. Phys. Chem. C* **2009**, *113*, 19208−19217.
(53) Chen, J.; Liang, T.; Li, J.; Wang, S.; Qin, Z.; Wang, P.; Huang, L.; Fan, W.; Wang, J. Regulation of Framework Aluminum Siting and Acid Distribution in H-MCM-22 by Boron Incorporation and Its Effect on the Catalytic Performance in Methanol to Hydrocarbons. *ACS Catal.* **2016**, *6*, 2299−2313.
(54) Ravel, B.; Newville, M. ATHENA, ARTEMIS, HEPHAESTUS: data analysis for X-ray absorption spectroscopy using IFEFFIT. *J. Synchrotron Radiat.* **2005**, *12*, 537−541.

https://doi.org/10.1021/acs.iecr.3c00988
Ind. Eng. Chem. Res. 2023, 62, 10939−10950